

TEMPERATURE AND PLASTIC STRAIN EVALUATION DURING FRICTION STIR REPAIR OF CORROSION DEFECTS IN AA2024

Original scientific paper

UDC:669.715:621.791.1
<https://doi.org/10.46793/aeletters.2025.10.1.3>Brahim Lakli^{1*}, Mohamed Berrahou¹, Mohamed Serier²¹Industrial Engineering and Sustainable Development Laboratory - GIDD, Faculty of Science and Technology, University of Relizane, Relizane, Algeria²Mechanical Engineering Department, University of Ain Temouchent, Ain Temouchent, Algeria

Abstract:

This paper presents a novel technique for repairing corrosion in aluminium plates, leveraging the principles of friction stir technology. The process employs a rotational speed of 1000 rpm and a traversal speed of 50 mm/min. The method involves applying a filling material to areas affected by pitting corrosion. A rotating tool generates frictional heat between the tool shoulder, filling material, and workpiece for a dwell time of several seconds, ensuring the softening of the material. As the tool traverses the corroded zone, the material is plastically deformed and deposited onto the damaged area. Additionally, a finite element simulation using a coupled Eulerian-Lagrangian approach predicts temperature distribution and mechanical deformation during the repair process for AA2024 aluminium plates, with all stages (plunging, dwelling, and mixing) simulated using ABAQUS/Explicit software. The results demonstrated that the repair method effectively filled all pitted areas on the corroded plate, achieving an excellent surface condition. The model accurately predicted the temperature distribution and the maximum temperature during the repair process, with the highest temperatures, up to 453°C (90% of the melting point of aluminium 2024), occurring directly under the tool shoulder. Additionally, the analysis revealed a maximum concentration of plastic strain in the same region, highlighting the localized impact of the repair technique.

ARTICLE HISTORY

Received: 27 October 2024
Revised: 29 January 2025
Accepted: 24 February 2025
Published: 31 March 2025

KEYWORDS

Friction stir processing, Corrosion repairing, AA2024, Aluminium alloy, Coupled Eulerian-Lagrangian, Finite element model, Temperature distribution

1. INTRODUCTION

Friction stir technologies have a long application history in both materials joining and processing [1-3]. Recent research is heavily focused on leveraging its proven effectiveness for defect repair in structural components [4, 5]. By leveraging the same principles of frictional heat generation, friction stir techniques can effectively repair defects like cracks, pores, inclusions, through holes, and grooves [6-8]. This innovative application has the potential to significantly improve the integrity and functionality of components in automotive, aerospace, and

shipbuilding, making it a valuable method for defect repair [9, 10].

Friction stir welding has been considered the most significant development in metal joining in a decade. Friction stir processing (FSP) was recently created to modify the microstructural properties of metallic materials. In research by Mishra and Ma [11], friction stir processing (FSP) was investigated as a technique to modify the microstructure and enhance the mechanical properties of aluminium alloys. Based on their analysis, it was found that FSP's refined grain structure and modified precipitation state resulted in significant improvements in the

*CONTACT: Brahim Lakli, e-mail: lakli.brahim@univ-relizane.dz

strength, hardness, and ductility of the aluminium alloys. Ultimately, their research demonstrated that friction stir processing is a useful technique for microstructural modification and performance enhancement of aluminium materials.

The research in [12] contributed to a better understanding of how FSP parameters influence processed materials' microstructure and mechanical properties, benefiting industries aiming to enhance surface properties without melting metals. Similarly, Elmetwally et al. [13] investigated the impact of friction stir welding (FSW) tool pin geometry on Al-Cu joints, demonstrating that a squared pin tool produced the strongest and most defect-free welds, while a triangular pin led to structural defects and brittle fractures. Their findings highlight the critical role of tool design in optimizing joint strength and microstructural integrity in solid-state welding processes.

Friction stir processing (FSP) was investigated as a technique to repair cracks in 304L stainless steel in a study by Miles et al. [14]. Their research demonstrated the effectiveness of FSP in repairing a tapered crack and a series of randomly sequenced cracks with different widths. They also investigated how the process affects the repaired area by testing its mechanical strength, hardness, and corrosion resistance. This study confirms that FSP can repair cracks.

In another study, friction stir processing (FSP) was examined by Ren et al. [15] for its ability to repair cracks in 2024 aluminium alloy. They combined experiments with simulations to analyse temperature, material flow, microstructure, and strength in the repaired zone. Their findings show that FSP repairs cracks in the solid state (without melting) by manipulating material flow and refining the grain structure. This leads to significant improvements in the tensile strength of the repaired area.

Avery et al. [16] demonstrated the effectiveness of additive friction stir deposition (AFS-D) as a solid-state repair method for high-strength aluminium alloys, highlighting its ability to restore mechanical integrity despite some variability in elongation and fatigue life. Building on the advancements in AFS-D, Mishra investigated the optimization of deposition quality using unsupervised machine learning [17]. By applying clustering algorithms such as k-means and autoencoders, the study identified intrinsic patterns in process parameters without requiring labelled data. The findings demonstrate that data-

driven approaches can enhance process control in AFS-D, improving quality and consistency, which is crucial for advancing solid-state additive manufacturing and repair techniques.

Friction stir technology is particularly advantageous for aluminium alloys commonly used in marine, automotive, and aerospace applications. In these industries, it is necessary to use materials that are strong, lightweight, and have excellent corrosion resistance. The 2024 and 2017 alloys from the 2xxx series are some of the most popular aluminium alloys because of their exceptional strength-to-weight ratio. However, they have a slightly lower corrosion resistance than other aluminium alloys.

Based on the basic principles of friction stir technology, a new technique for repairing corrosion has been developed. By applying filler material to the corroded area, the rotating tool generated heat through friction, fusing the filler material with the base metal.

In this study, a friction stir technique for repairing corrosion, which was a variant of the friction stir technologies, was proposed to repair the corrosion defects. We used a finite element simulation with a coupled Eulerian-Lagrangian formulation to predict the temperature distribution and mechanical deformation during the friction stir process for repairing the corrosion of 2024 aluminium plates.

2. MATERIAL AND METHODS

The repair process for pitting corrosion involves several steps, as illustrated in the schematic in Fig. 1. A conventional milling machine was used to perform the experiments of the friction stir technique for corrosion repair. The Workpiece material used in the present study was aluminium alloy AA2024 with a dimension of 140x60x3 mm³ (Fig. 2). The chemical composition (%wt) of the alloy is as follows: silicon (Si) at 0.5%, iron (Fe) at 0.5%, copper (Cu) ranging from 3.8% to 4.9%, manganese (Mn) between 0.3% and 1.0%, magnesium (Mg) from 1.2% to 1.8%, chromium (Cr) at 0.1%, zinc (Zn) at 0.25%, titanium (Ti) at 0.15%, and aluminium (Al) in balance [18]. The plates are immersed in a 10% sodium chloride (NaCl) solution for 25 days to perform a corrosion test on the aluminium. The plates were regularly inspected for signs of corrosion. The number of pits increases over time, showing the propagation of pitting corrosion. The depth of the pits also increased, with the average pit depth reaching 0.3

mm. The repair method utilizes a pinless tool crafted from H13 steel with a shoulder diameter of 12 mm (Fig. 3) and a specific chemical composition as specified in [19, 20]. According to these references, H13 contains 0.32–0.45 wt% Carbon (C), 0.20–0.50 wt% Manganese (Mn), 0.80–1.20 wt% Silicon (Si), 4.75–5.50 wt% Chromium (Cr), a maximum of 0.30 wt% Nickel (Ni), 1.10–1.75 wt% Molybdenum (Mo), and 0.80–1.20 wt% Vanadium (V) [19, 20]. ER4043, with a diameter of 3 mm, was selected as the filling material, and its chemical composition is specified in [21]. ER4043 consists primarily of Aluminium (Al) at 93.43 wt%, with Silicon (Si) at 5.25 wt%, Iron (Fe) at 0.80 wt%, Copper (Cu) at 0.30 wt%, Manganese (Mn) at 0.05 wt%, Magnesium (Mg) at 0.05 wt%, Zinc (Zn) at 0.10 wt%, and Titanium (Ti) at 0.02 wt% [21]. The process employs a rotational speed of 1000 rpm and a traversal speed of 50 mm/min. Plunging, dwelling, and mixing were all steps in the repair procedure.

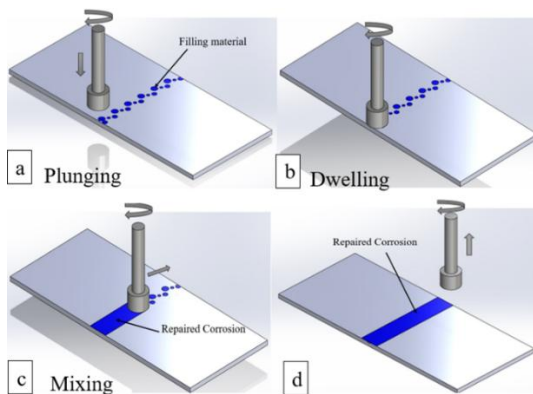


Fig. 1. Schematic of the repairing corrosion process

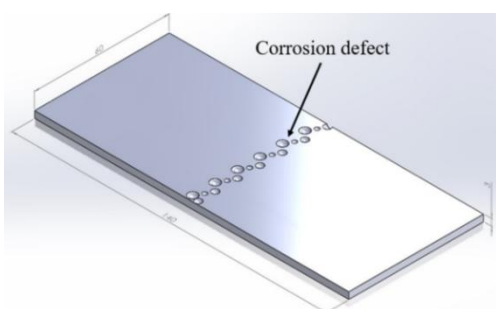


Fig. 2. Geometry of the workpiece

Firstly, the metal surface should be clean. Second, the filling material is applied to the area affected by pitting corrosion (as shown in Fig. 1a). The rotating tool exerted frictional heat on the filling material and workpiece for a dwell time of several seconds (Fig. 1b), this produces the frictional heat between the tool shoulder, filling material, and workpiece, ensuring softening of the material. Then, the tool traverses along the

corrosion-affected zone, the material is plastically deformed, and it starts getting deposited on the corroded zone (Fig. 1c). In the end, the pitting corrosion defect was repaired, and the tool was retracted (Fig. 1d).

During the experiments, the temperature was measured to ensure sufficient melting of the filler material for bonding with the base metal. The initial temperature of the tool and workpiece was 25°C.

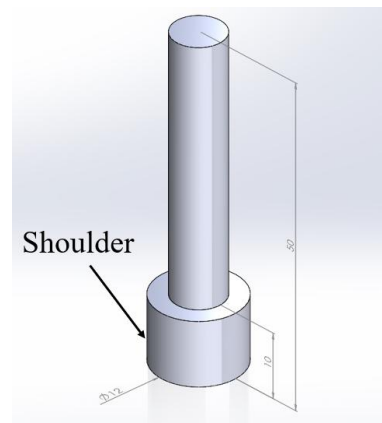


Fig. 3. Geometry of the tool

3. FINITE ELEMENT MODEL

The Coupled Eulerian-Lagrangian (CEL) technique available in ABAQUS was used to predict the temperature distribution during the friction stir repairing corrosion of AA2024 plates. The model consists of a stationary (140x60x3 mm³) plate of AA2024 and a moving FS tool.

3.1 Material Model

A three-dimensional coupled thermo-mechanical finite element model based on the Coupled Eulerian-Lagrangian (CEL) approach using an explicit algorithm has been developed in ABAQUS to simulate the friction stir process to repair corrosion (plunging, dwelling, and mixing steps) and predict thermal history.

Friction stir repairing corrosion is a large material deformation technique that is difficult to solve using the Lagrangian and Eulerian methods. Consequently, the workpiece is considered as a coupled Eulerian and Lagrangian body, while the tool is defined as a Lagrangian body.

The 3D part model of the aluminium alloy 2024 plate with dimensions 140mm x 60mm x 3mm and H13 tool steel have been drawn for the friction stir repairing corrosion simulation, as shown in Figs. 4 and 5.

The Eulerian domain geometry was simulated as a local domain with dimensions 140mm x 60mm x 8mm. The local domain consisted of two regions, as shown in Fig. 6. The bottom region is the material region (blue colour), with a thickness of 3 mm (equal to the plate thickness used in the experimental work) and assigned the properties of the base metal (AA 2024). The upper region is the material-free region (green colour), which has a thickness of 5 mm and is left empty with no material properties.

The material properties of AA2024 and H13 tool steel for the FE simulation are specified in [22, 23]. According to these references, AA 2024 has a density of 2700 kg/m³, a thermal conductivity of 190 W/m·K, a Young's modulus of 70 GPa, a Poisson's ratio of 0.3, and a specific heat of 900 J/kg·K [22]. H13 tool steel has a density of 7800 kg/m³, a thermal conductivity of 24.5 W/m·K, a Young's modulus of 210 GPa, a Poisson's ratio of 0.3, and a specific heat of 278 J/kg·K [23]. The Johnson Cook material model [24], which depicts the flow stress of material as a function of temperature and rate of deformation, has been used to define the plasticity behaviour of materials, as shown in Eq. (1).

$$\sigma_{flowstress} = (A + B \varepsilon^n) \left[1 + C \ln \left(1 + \frac{\dot{\varepsilon}}{\dot{\varepsilon}_0} \right) \right] \left[1 - \left(\frac{T - T_{room}}{T_{melt} - T_{room}} \right)^m \right] \quad (1)$$

where are:

$\sigma_{flowstress}$ - is a flow stress,
 $\dot{\varepsilon}$, ε and $\dot{\varepsilon}_0$ - represent effective strain, strain rate and reference strain rate, respectively,
 A - represents the material yield stress,
 B - represents the strain factor,
 C - represents strain rate factor,
 n - represents strain exponent,
 m - represents Temperature exponent,
 T_{melt} , T_{room} and T represent the melting temperature, room temperature and transition temperature, respectively.

The Johnson-Cook material properties for AA 2024 are specified in [22]. According to this reference, the yield stress constant (A) is 352 MPa, the strain factor (B) is 440 MPa, the strain rate factor (C) is 0.0083, the temperature exponent (m) is 1.7, and the strain exponent (n) is 0.42. Additionally, the melting temperature (T_{melt}) is 775 K, and the room temperature (T_{room}) is 293 K [22].

After part modeling, the simulation method (dynamic temp displacement), simulation time, and simulation steps such as plunging, dwelling, and mixing have been fixed. The Fourier rule of heat conduction governs the heat produced at the

frictional contact of the tool and workpiece during the friction stir modeling, as shown in Eq. (2) [25].

$$k \left[\frac{\partial^2 T}{\partial x^2} + \frac{\partial^2 T}{\partial y^2} + \frac{\partial^2 T}{\partial z^2} \right] + \dot{q} = \rho c \frac{\delta T}{\delta t} \quad (2)$$

where are:

k - is the thermal conductivity,
 ρ - is the density of the material,
 C - is specific heat capacity,
 t - is time,
 q - is heat generation rate.

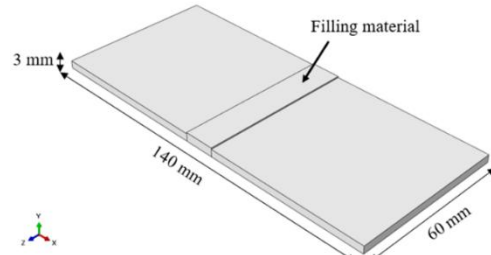


Fig. 4. The 3D part model of aluminum plate

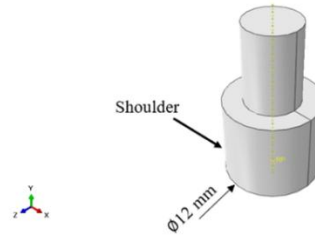


Fig. 5. The 3D part model of tool

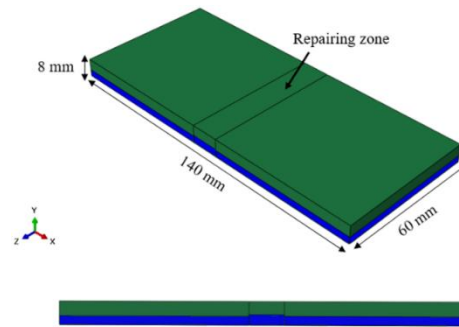


Fig. 6. The 3D part model of Eulerian domain

3.2 Boundary Condition

The boundary conditions play a critical role in the finite element study. The thermal and mechanical boundary conditions are applied to replicate the experimental condition in the simulation model, as shown in Fig. 7. The boundary conditions used are as follows:

- During the friction stir process, the workpiece was constrained to move in the x, y, and z

directions by the appropriate boundary condition.

- Tool rotation speeds of 1000 RPM were applied.
- The three steps of the simulation were divided. Step 1 consisted of the plunging period, step 2 consisted of the dwelling period, and step 3 consisted of the mixing period.
- The heat dissipation between the backing plate and the bottom surface of the workpiece is measured using the convective heat transfer coefficient, which has a value of $1000 \text{ W/m}^2\text{C}$ [26].
- The heat transfer involved between the workpiece and environment has been characterized by the convective boundary condition on the top and side surfaces of the workpiece and the convective coefficient with a value of $10 \text{ W/m}^2\text{C}$ [26].
- The temperature distribution to the workpiece and tool has been calculated using the predefined field boundary condition.
- A temperature of 25°C was assumed for the room throughout the friction stir corrosion repair process. This implies that the tool and workpiece temperatures were at room temperature values during the initial operation stage.
- The general contact algorithm is used to define all incorporated contacts between the workpiece and tool. Which is defined by a friction law for tangential behaviour and a "hard contact" for normal behaviour.
- A frictional coefficient value of 0.4 was assumed.
- Frictional and plastic dissipation energy were identified as the sources of heat generation during the friction stir technique. 100% of the frictional energy dissipation was assumed to be converted to heat. 90% of the plastic work was considered to be converted to heat.

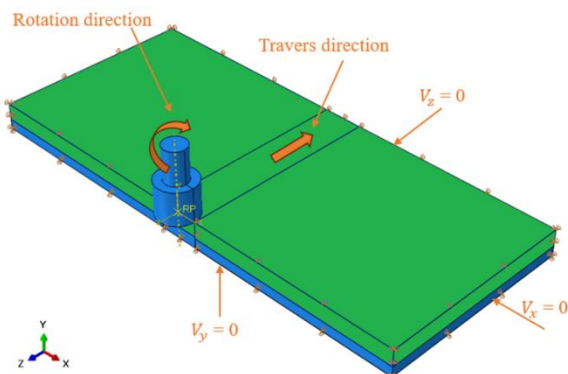


Fig. 7. Boundary conditions used in the CEL model

3.3 Mesh Details

Through contact interaction, the Eulerian body is related to the Lagrangian. The Eulerian frame is used to discredit the workpieces, and the Lagrangian reference frame is used to discredit the tool. Coupled Eulerian-Lagrangian (CEL) analysis is the term used to describe simulations using this kind of interaction (Fig. 8). The Lagrangian mesh is attached to the material points. As the material deforms, the mesh deforms with it. The Eulerian mesh serves as a background grid in contrast. The mesh stays the same as the material deforms (or flows) inside the mesh. The extent of deformation, in this case, is measured when the material particle flows across an element node.

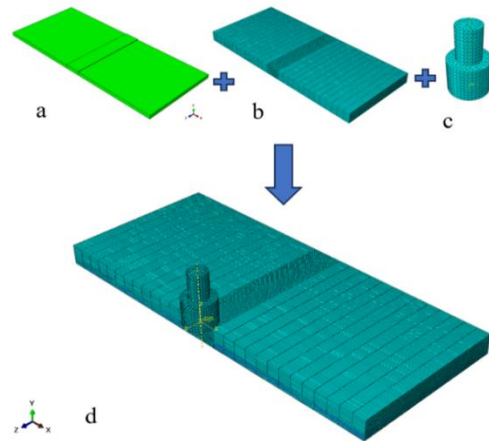


Fig. 8. The full mesh: a) Workpiece (Reference), b) Eulerian domain, c) Tool, d) coupled Eulerian-Lagrangian

Eulerian analysis is highly effective for applications involving extreme deformation, such as fluid flow. In these applications, Lagrangian analysis methods encounter limitations due to significant mesh distortion and resulting loss of accuracy. During the friction stir corrosion repair process, materials enter a viscous state. This viscous state can be efficiently described using Eulerian analysis.

Abaqus/Explicit uses a volume-of-fluid method for its Eulerian implementation to track material flow through the mesh. This is done by computing the Eulerian volume fraction (EVF) within each element. This fraction represents the portion of the element filled by the material. Simply put, a value of 1 indicates the element is completely full, and 0 means it's empty. In our analysis, we employ the multi-material, thermally coupled element type EC3D8RT. Within the Coupled Eulerian-Lagrangian Formulation, the volume fraction tool uses the parts to be repaired as a volume

reference in the Eulerian domain. A key advantage of this method is that the parts to be repaired do not require meshing, only the Eulerian domain needs to mesh.

The full mesh adopted for the workpiece and the tool is shown in Fig. 8. The tool was meshed using a four-node linear displacement and temperature-coupled element (C3D4T).

4. RESULTS AND DISCUSSION

4.1 Experimental Results

The corroded plate before repair is shown in Fig. 9a. The surface exhibits pitting, a type of localized corrosion characterized by small holes. A filler material was applied to the affected area to repair this pitting corrosion. A rotating tool then generated heat through friction, fusing the filler material with the base metal.

Precise temperature control was essential to ensure the filler material melted adequately for bonding with the base metal. The maximum temperature of friction stir repairing corrosion at the plate interface (420°C) was measured in the experimental work in the mixing stage.

As demonstrated in Fig. 9b, the repair process was successful, completely filling the pitted areas of the plate, achieving a high-quality surface condition.

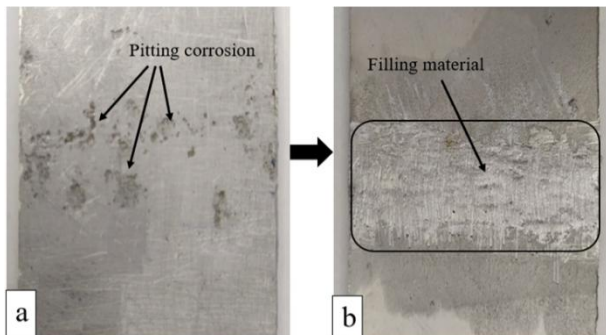


Fig. 9. Corrosion repairing: a) before repairing, b) after repairing

4.2 Temperature Distribution

The simulation model results are depicted as temperature distributions obtained from the finite element simulation of friction stir repairing corrosion. In this simulation, boundary conditions, mesh generation, and specified material modeling are all involved. The cross-sectional views of the workpiece's temperature distribution during the plunging, dwelling and mixing stages are depicted in Figs. 10a, 10b and 10c. In the plunging stage, the

temperature is low, and during the dwelling and mixing stages, it gradually rises. Over time, the friction between the tool shoulder and the workpiece surface increases, producing more heat generation, which is why the mixing stage displays the biggest temperature distribution region. Additionally, the overall temperature distribution of the friction stir repairing simulation in a 3D view is illustrated in Fig. 10d, providing a comprehensive visualization of the heat-affected zone.

The simulation results indicate a peak temperature of 450°C at the centre of the repair zone, corresponding to the interface between the tool and workpiece. This temperature gradually decreases as the distance from the centre of the repair zone increases.

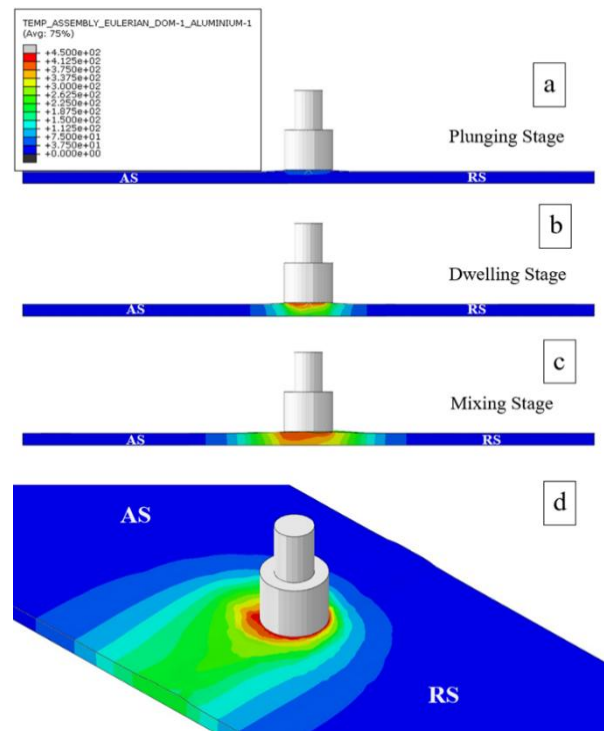


Fig. 10. (a), (b) and (c) Cross-sectional views of the workpiece's temperature distribution in the plunging stage, dwelling stage and mixing stage, respectively, (d) Temperature distribution of friction stir repairing simulation

4.2.1 Temperature Evolution as a Function of Distance

For observing the temperature distribution throughout the workpiece, the graphs plot the temperature on the y-axis and the distance from the centre of the repair zone on the x-axis, as shown in Figs. 11 and 13, which shows how the temperature varies across the workpiece.

The temperature values obtained by simulation were taken from nodes placed on a line perpendicular to the repair zone (Fig. 12) and on a line along the thickness of the plate (Fig. 14).

Fig. 11 shows the temperature distribution along the lateral direction, perpendicular to the repair line at the plunging, dwelling and mixing stages. The zone directly under the tool shoulder experiences the highest temperatures due to concentrated frictional heat and plastic deformation during the repair process. Interestingly, the advancing side (AS) generally exhibits a hotter profile than the retreating side (RS). This can be attributed to the stirring action of the tool, which generates additional friction and, consequently, more heat on the advancing side. This effect is reflected in the slightly higher peak temperature recorded on the AS, reaching up to 453°C, a value approaching 90% of the melting point for AA 2024 aluminium. The temperature progressively decreases with increasing distance from the repair zone on both sides. This creates distinct thermal and mechanical influence zones within the repair cross-section. The material towards the end of the workpiece experiences minimal thermal impact, with temperatures approaching ambient levels, signifying minimal thermal or mechanical changes in this region.

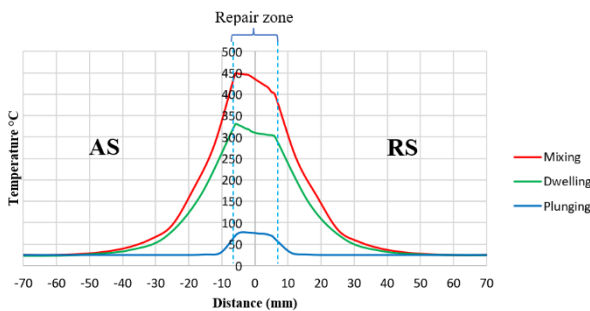


Fig. 11. The temperature distribution along the lateral direction

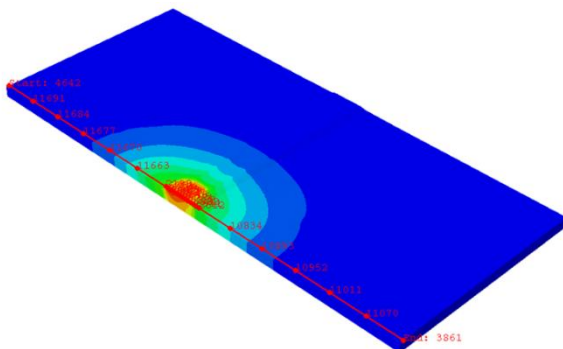


Fig. 12. The path of the nodes along the lateral direction perpendicular to the repair zone

Fig. 13 shows the temperature distribution along the vertical direction at the dwelling and mixing stages. The highest temperatures are observed directly under the tool shoulder at the top surface. This region experiences the brunt of frictional heat generation. The temperature then gradually decreases as it travels through the middle section of the material and finally reaches the bottom surface. This observed gradient reflects the combined influence of concentrated heat generation at the top by the tool shoulder and heat conduction through the material.

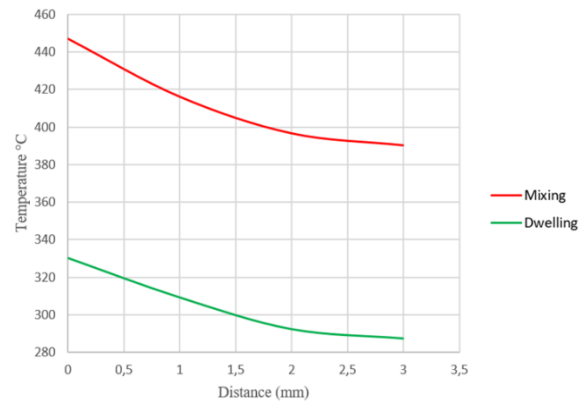


Fig. 13. The temperature distribution along the vertical direction



Fig. 14. The path of the nodes along the vertical direction

4.2.2 Temperature Evolution as a Function of Time

Fig. 15 shows the evolution of the temperature as a function of time. The temperature values obtained by simulation were taken from a node placed at the beginning of the workpiece on the repair zone, as shown in Fig. 16. Initially, the material has a temperature of 25°C. This is the ambient temperature considered in the simulation. During the plunging phase, the rotating tool contacts the material, creating friction and heat. In the dwelling phase, the rotating tool remains stationary in the repair zone (without traversal), causing a quick increase in temperature at the contact surface. During the mixing phase, the temperature continues to rise until it reaches a peak. The highest temperature achieved during friction stir repairing corrosion can reach 453°C, corresponding to 90% of the

melting point of the aluminium alloy 2024. As the tool moves forward, the temperature gradually decreases behind it. The rate of decrease depends on the heat conduction properties of the workpiece material. Heat dissipates into the material and surrounding environment as the tool advances.

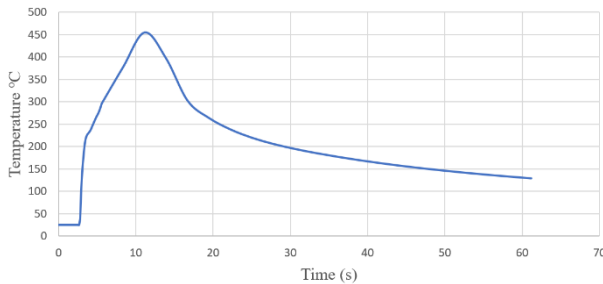


Fig. 15. The evolution of the temperature as a function of time

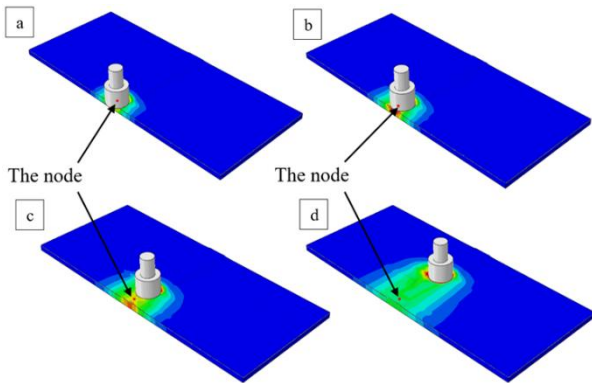


Fig. 16. Position of the node at different times

4.3 Plastic Strain Distribution

Fig. 17 shows a plastic strain distribution as a function of distance from the centre of the tool (perpendicular to the repair line). Finite element analysis (FEA) reveals a concentration of plastic strain within the repair zone at the top surface of the plate. This localization is attributed to the intense material flow and mixing induced by the rotating tool. The highest strain level is concentrated directly under the tool shoulder, where the combination of high pressure and torque generates significant heat. This heat, in turn, plays a major role in plasticizing the material. Interestingly, the analysis shows a clear asymmetry in strain distribution, with the advancing side (AS) experiencing a greater degree of plastic deformation compared to the retreating side (RS). This asymmetry is likely a consequence of the material deposition process. The plastic strain distribution exhibits a significant decrease with increasing distance from the repair zone on both sides, eventually reaching zero at the

workpiece edge, which signifies the region unaffected by the repair process.

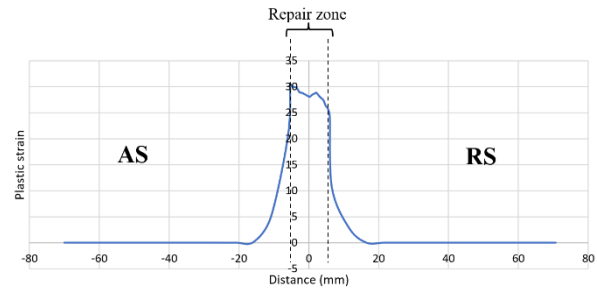


Fig. 17. Plastic strain distribution as a function of distance from the centre of the tool

5. CONCLUSION

In this work, A recent advancement in friction stir technology demonstrates a successful method for repairing corrosion defects in aluminium plates. This method achieves the repair by using a pinless tool and a filler material. Frictional heat is generated by the rotating tool on the workpiece and filler material. This heat is produced by plastic dissipation and friction, which allows the filler material to fuse with the base metal to repair the corrosion.

A 3D finite element analysis utilizing the Coupled Eulerian-Lagrangian (CEL) method was employed to simulate the process response during friction stir repair of corrosion defects in Al 2024 alloy. This comprehensive simulation, implemented within ABAQUS/Explicit software, encompassed all three stages of the repair process: plunging, dwelling, and mixing. Measuring the temperature distribution and frictional heat generation at the contact between the tool and the workpiece, particularly under the shoulder, is practically problematic. Therefore, the simulation model offers an alternative for predicting temperature in this region. Based on this analysis, the following conclusions can be drawn from the study:

- From a visual examination of the repaired plate in the experimental results, it can be concluded that the repair process was successful, completely filling the pitted area of the corroded plate and achieving a high-quality surface condition.
- The maximum temperature of friction stir repairing corrosion at the plate interface (420°C) was measured in the experimental work in the mixing stage.
- Finite element analysis results validate the model's ability to accurately predict the

temperature distribution and maximum temperature during friction stir repair of corrosion.

- The temperature rises due to friction between the tool and the material.
- The highest temperatures are observed directly under the tool shoulder, and this temperature gradually decreases with the increasing distance from the repair zone on both sides.
- The temperature gradually decreases from top to bottom in the direction of the thickness.
- The highest temperature achieved during friction stir repairing corrosion can reach 453°C, corresponding to 90% of the melting point of the aluminium alloy 2024.
- Analysis of plastic strain reveals a maximum concentration directly under the tool shoulder, with a significant decrease observed as the distance from the repair zone increases on both sides. This phenomenon is attributed to the intense mixing and material flow generated by the rotating tool within the repair zone.
- Analysis revealed an asymmetry in the thermal profile, with the advancing side (AS) exhibiting a more extensive high-temperature zone compared to the retreating side (RS). This difference in thermal exposure is reflected in the plastic strain distribution, with the AS experiencing higher strain values compared to the RS.

The finite element (FE) model with the CEL approach successfully captures both thermal history and plastic deformation during friction stir repair of corrosion, demonstrating its effectiveness for simulating multi-physics problems. Future research will leverage this FE model to optimize the parameters of the friction stir process for repairing corrosion.

CONFLICTS OF INTEREST

The authors declare no conflict of interest.

REFERENCES

- [1] N.E. El-Zathry, S. Akinlabi, W.L. Woo, V. Patel, R.M. Mahamood, Friction stir-based techniques: an overview. *Welding in the World*, 69, 2024: 1-35. <https://doi.org/10.1007/s40194-024-01847-w>
- [2] L.E. Murr, Friction-stir welding and processing. *Handbook of Materials Structures, Properties, Processing and Performance*. Springer, Cham, 2017. https://doi.org/10.1007/978-3-319-01905-5_51-2
- [3] D.A.P. Prabhakar, A.K. Shettigar, M.A. Herbert, M.G.C. Patel, D.Y. Pimenov, K. Giasin, C. Prakash, A comprehensive review of friction stir techniques in structural materials and alloys: challenges and trends. *Journal of materials research and technology*, 20, 2022: 3025-3060. <https://doi.org/10.1016/j.jmrt.2022.08.034>
- [4] N. Maddela, M. Aluri, M.D. Jakirahemed, Study on defects repairing using Friction Stir technologies. *Materials Today: Proceedings*, 44, 2021: 2373-2379. <https://doi.org/10.1016/j.matpr.2020.12.441>
- [5] L.P. Martin, A. Luccitti, M. Walluk, Repair of aluminum 6061 plate by additive friction stir deposition. *The International Journal of Advanced Manufacturing Technology*, 118, 2022: 759-773. <https://doi.org/10.1007/s00170-021-07953-z>
- [6] M. Sajed, S.M.H. Seyedkashi, Multilayer friction stir plug welding: A novel solid-state method to repair cracks and voids in thick aluminum plates. *CIRP Journal of Manufacturing Science and Technology*, 31, 2020: 467-477. <https://doi.org/10.1016/j.cirpj.2020.07.009>
- [7] R. Huang, S. Ji, X. Meng, Z. Li, Drilling-filling friction stir repairing of AZ31B magnesium alloy. *Journal of Materials Processing Technology*, 255, 2018: 765-772. <https://doi.org/10.1016/j.jmatprotec.2018.01.019>
- [8] R.J. Griffiths, D.T. Petersen, D. Garcia, H.Z. Yu, Additive friction stir-enabled solid-state additive manufacturing for the repair of 7075 aluminum alloy. *Applied Sciences*, 9(17), 2019: 3486. <https://doi.org/10.3390/app9173486>
- [9] Z. Lv, S. Han, W. Hu, Z. Dong, R. Huang, K. Yang, Solid-State Repair of Casting Defects in ZL210 Aluminum Alloy. *Journal of Materials Engineering and Performance*, 29, 2020: 5886-5893. <https://doi.org/10.1007/s11665-020-05054-8>
- [10] R.A. Kumar, R.G.A. Kumar, K.A. Ahamed, B.D. Alstyn, V. Vignesh, Review of friction stir

- processing of aluminium alloys. *Materials Today: Proceedings*, 16, 2019: 1048-1054.
<https://doi.org/10.1016/j.matpr.2019.05.194>
- [11] R.S. Mishra, Z.Y. Ma, Friction stir welding and processing. *Materials science and engineering: R: reports*, 50(1-2), 2005: 1-78.
<https://doi.org/10.1016/j.mser.2005.07.001>
- [12] M.S. Węglowski, Experimental study and response surface methodology for investigation of FSP process. *Archive of Mechanical Engineering*, 61(4), 2014: 539-552.
<https://doi.org/10.2478/meceng-2014-0031>
- [13] H.T. Elmetwally, M.A. Abdelhafiz, M.N. El-Sheikh, M.E. Abdullah, Effect of friction stir welding tool pin geometry on the characteristics of Al-Cu joints. *Applied Engineering Letters*, 8(2), 2023: 60-69.
<https://doi.org/10.18485/aeletters.2023.8.2.3>
- [14] M.P. Miles, C. Gunter, F. Liu, T.W. Nelson, Friction Stir Processing of 304L Stainless Steel for Crack Repair. In: Hovanski, Y., Mishra, R., Sato, Y., Upadhyay, P., Yan, D. (eds) *Friction Stir Welding and Processing IX. The Minerals, Metals & Materials Series. Springer*, Cham, 2017: 13-22.
https://doi.org/10.1007/978-3-319-52383-5_2
- [15] J.G. Ren, L. Wang, D.K. Xu, L.Y. Xie, Z.C. Zhang, Analysis and modeling of friction stir processing-based crack repairing in 2024 aluminum alloy. *Acta Metallurgica Sinica (English Letters)*, 30, 2017: 228-237.
<https://doi.org/10.1007/s40195-016-0489-8>
- [16] D.Z. Avery, C.E. Cleek, B.J. Phillips, M.Y. Rekha, R.P. Kinser, H.M. Rao, L.N. Brewer, P.G. Allison, J.B. Jordon, Evaluation of microstructure and mechanical properties of Al-Zn-Mg-Cu alloy repaired via additive friction stir deposition. *Journal of Engineering Materials and Technology*, 144(3), 2022: 031003.
<https://doi.org/10.1115/1.4052816>
- [17] A. Mishra, Deposition Quality Optimization of Additive Friction Stir Deposited Aluminium Alloy Using Unsupervised Machine Learning. *Advanced Engineering Letters*, 3(2), 2024: 52-63.
<https://doi.org/10.46793/adeletters.2024.3.2.2>
- [18] H. Chen, S. Liu, P. Wang, X. Wang, Z. Liu, F. Aldakheel, Effect of grain structure on fatigue crack propagation behavior of 2024 aluminum alloy under different stress ratios. *Materials & Design*, 244, 2024: 113117.
<https://doi.org/10.1016/j.matdes.2024.113117>
- [19] J.R. Davis (Ed.), *Carbon and alloy steels. Materials Park, OH: Asm International*, 1996.
- [20] J. Marashi, E. Yakushina, P. Xirouchakis, R. Zante, J. Foster, An evaluation of H13 tool steel deformation in hot forging conditions. *Journal of Materials Processing Technology*, 246, 2017: 276-284.
<https://doi.org/10.1016/j.jmatprotec.2017.03.026>
- [21] R.P. Verma, K.N. Pandey, Y. Sharma, Effect of ER4043 and ER5356 filler wire on mechanical properties and microstructure of dissimilar aluminium alloys, 5083-O and 6061-T6 joint, welded by the metal inert gas welding. *Proceedings of the Institution of Mechanical Engineers, Part B: Journal of Engineering Manufacture*, 229(6), 2015: 1021-1028.
<https://doi.org/10.1177/0954405414535771>
- [22] M. Rodriguez-Millan, D. Garcia-Gonzalez, A. Rusinek, A. Arias, Influence of stress state on the mechanical impact and deformation behaviors of aluminum alloys. *Metals*, 8(7), 2018: 520.
<https://doi.org/10.3390/met8070520>
- [23] R. Jain, S.K. Pal, S.B. Singh, 5- Numerical modeling methodologies for friction stir welding process. *Computational methods and production engineering*, Woodhead Publishing, 2017: 125-169.
<https://doi.org/10.1016/B978-0-85709-481-0.00005-7>
- [24] K.C. Jorgensen, V. Swan, Modeling of armour-piercing Projectile Perforation of thick aluminium plates. *Proceedings of the 13th International LS-DYNA Conference*, June 2014, Detroit, MI, USA.
- [25] A.J.M. Spencer, *Continuum Mechanics*. Courier Corporation. *Longman*, New York, 2012.
- [26] K.N. Salloomi, F.I. Hussein, S.N.M. Al-Sumaidae, Temperature and Stress Evaluation during Three Different Phases of Friction Stir Welding of AA 7075-T651 Alloy. *Modelling and Simulation in Engineering*, 2020(1), 2020: 3197813.
<https://doi.org/10.1155/2020/3197813>